Effect of charged dislocation scattering on electrical and electrothermal transport in *n*-type InN

Nate Miller and Eugene E. Haller

Materials Sciences Division, Lawrence Berkeley National Laboratory, Berkeley, California 94720, USA and Department of Materials Science and Engineering, University of California, Berkeley, California 94720, USA

Gregor Koblmüller

Physik Department and Walter Schottky Institut, Technische Universität München, Am Coulombwall 3, D-85748 Garching, Germany

Chad Gallinat and James S. Speck

Materials Department, University of California, Santa Barbara, California 93106, USA

William J. Schaff

Dept. of Electrical and Computer Engineering, Cornell University, Ithaca, New York 14853, USA

Michael E. Hawkridge, Kin Man Yu, and Joel W. Ager III[*]

Materials Sciences Division, Lawrence Berkeley National Laboratory, Berkeley, California 94720, USA

(Received 31 January 2011; revised manuscript received 21 April 2011; published 9 August 2011)

Temperature-dependent thermopower and Hall-effect measurements, combined with model calculations including all of the relevant elastic- and inelastic-scattering mechanisms, are used to quantify the role of charged line defects on electron transport in *n*-type InN films grown by molecular-beam epitaxy. Films with electron concentrations between 4×10^{17} and 5×10^{19} cm^{-3} were investigated. Charged point and line defect scattering produce qualitatively different temperature dependences of the thermopower and mobility, allowing their relative contribution to the scattering to be evaluated using charge neutrality at the measured electron concentration. Both charge state possibilities for the dislocations [positively charged (donors) or negatively charged (acceptors)], were considered. The 100–300 K temperature dependence of the mobility and the 200–320 K temperature dependence of the thermopower can be modeled well with either assumption. The dislocation density was independently measured by plan-view and cross-sectional transmission electron microscopy and corresponds well with the values obtained from transport modeling.

DOI: 10.1103/PhysRevB.84.075315 PACS number(s): 72.20.−i, 73.61.Ey, 73.50.Lw

I. INTRODUCTION

InN has a narrow band gap of close to 0.65 eV and a small electron effective mass.[1,2] The estimated LO-phonon limited room-temperature mobility is predicted to be in excess of 10 000 cm^2 V^{-1} s^{-1},[3,4] which would be of interest for high-speed device applications.[5] There have been concerted efforts using molecular-beam epitaxy (MBE), metalorganic vapor phase epitaxy (MOVPE), and other growth methods to produce high-quality InN thin films.[6] However, the low electron concentrations, $< 10^{16}$ cm^{-3}, which would be required to produce high mobility material, have not been achieved. To date, the lowest reported electron concentrations n for InN thin films are in the low 10^{17} cm^{-3} range, with mobilities approaching 2500 cm^2 V^{-1} s^{-1}.[7]

There is considerable discussion in the literature about the source of the unintentional background electron concentration. Some studies have found a correlation between the electron concentration n and impurity concentrations, most notably hydrogen and oxygen.[7–9] While it might appear surprising that hydrogen can be a donor in InN, this assignment is well supported by first-principles calculations.[10,11] Other studies have found that dislocations function as donors and are the source of at least some of the electrons.[12–14]

There is also an active discussion of what is mobility limiting in these films: ionized impurities (singly or multiply charged) and/or ionized line defects such as dislocations. Because InN growth is exclusively heteroepitaxial, usually on GaN, threading dislocation (TD) densities in InN are very high, typically in the range of 10^9–10^{11} cm^{-2}.[15–17] It is clear at least qualitatively that dislocations play a role in limiting electron transport in *n*-type InN. For example, studies of nonradiative recombination[18] and of electron transport (mobility)[14,19,20] have found deleterious effects, which are attributed to charged dislocations.

It is well established that charged dislocations affect mobility in the related III-nitride compound, GaN.[21] In GaN films, there is considerable experimental evidence from electron holography[22,23] and scanning probe microscopy[24–27] that dislocations are negatively charged, consistent with acceptor behavior. At high densities, the dislocations scatter carriers, reducing the mobility.[21] Following the analogy with GaN, some studies have investigated the effect of charged dislocations on electron mobility in InN, assuming them to be acceptors.[28–30] However, the experimental studies mentioned above,[12–14] and a recent *ab initio* calculation,[31] provide evidence that dislocations in InN can be donors.

Here we present an experimental electrothermal transport study of InN thin films. In addition to measuring n and $\mu(T)$ via the Hall effect, as is standard, we also measured the thermopower (Seebeck coefficient S) and find that this additional measurement provides considerable discernment as to the details of the electron scattering. We also calculated

 ©2011 American Physical Society

$\mu(T)$ and $S(T)$ by solving the Boltzmann transport equation, incorporating all the relevant scattering mechanisms including charged dislocations. Under the assumption of charge neutrality, we fit the transport data using the dislocation density as the main adjustable parameter. Both cases mentioned above regarding the charge state, positive or negative, are considered. The dislocation density we extract from the transport modeling is in good agreement with values obtained by transmission electron microscopy (TEM).

II. EXPERIMENTAL

Films grown by MBE were used in this study, as this technique has achieved the lowest electron concentrations and highest 300 K mobilities in InN films to date. InN thin film samples grown at Cornell University and at the University of California, Santa Barbara (UCSB) were used for this work. The Cornell samples were grown on *c*-sapphire substrates using AlN nucleation and GaN buffer layers.[32,33] The UCSB samples were grown by plasma assisted MBE (PAMBE) on semi-insulating GaN commercial templates using ∼100 nm thick undoped GaN buffer layers.[34,35] In all films, the GaN and other buffer layers were sufficiently insulating to have negligible contributions to the electrical and thermopower measurements.

Hall-effect measurements were measured as a function of temperature from 10 to 300 K using a 3000 Gauss magnet and contacts placed in the van der Pauw configuration. Thermopower measurements were performed from 180 to 340 K using a system which has been described previously.[36,37] The measurements were performed on a large sample set with n ranging from 4×10^{17} to 5×10^{19} cm^{-3}. InN is degenerate within this electron concentration range and little change of n with temperature was observed. A summary of the Hall effect and Seebeck coefficients for these films is shown in Table I. The composition and thickness of the films were determined by Rutherford backscattering spectrometry (RBS). Scanning electron microscopy was used to measure the thickness of thicker films. Detailed TEM measurements were performed on three of the films in the study. Dislocation densities were determined using two-beam conditions and the invisibility criterion in both plan-view and cross-sectional geometries.

III. THEORY

The mobility μ and Seebeck coefficient S were calculated by solving the Boltzmann transport equation using Rode's iterative method.[38,39] An overview of the approach will be given here; further details are in the Appendix. The standard carrier scattering mechanisms for polar semiconductors were included in the calculations but only ionized impurity, line charge (due to dislocations), and LO phonon scattering made significant contributions to the overall scattering over the experimental temperature range.

TABLE I. Experimentally measured film thickness d, electron concentration n, mobility μ, and Seebeck coefficient S for the three films examined in detail in this study. The transport data are for room temperature.

Sample	d (nm)	n (cm^{-3})	μ (cm^2/V s)	S (μV/K)
A (GS1360)	128	6×10^{18}	364	−86
B (100907AC)	1000	9×10^{17}	654	−194
C (GS2060)	12160	4×10^{17}	1191	−227

TABLE II. Summary of physical parameters and constants for wurtzite InN used in the transport calculations. Values are taken from Ref. 46 unless noted otherwise.

Parameter	Value
Band gap (eV)	0.65[a]
Band-edge electron effective mass, $m^*_{e,0}/m_0$	0.055[b]
LO phonon energy (meV)	73
Static dielectric constant, $\varepsilon_S/\varepsilon_0$	10.3[c]
High frequency dielectric constant, $\varepsilon_\infty/\varepsilon_0$	6.7
Volume deformation potential (eV)	3.6
Acoustic phonon velocity, longitudinal (cm/s)	5.2×10^5
Acoustic phonon velocity, transverse (cm/s)	1.2×10^5
Piezoelectric constant, e_{14} (C/m^2)	0.375
c lattice constant (nm)	0.57038[d]

[a]From Ref. 47.
[b]From Ref. 2.
[c]From Ref. 42.
[d]From Ref. 48.

The choice of the band-edge effective mass merits discussion. Many measurements of the band-edge effective masses for wurtzite InN are in the range of 0.05–0.08m_0,[2,40–42] although there are reports of higher values.[43–45] Here we use the value 0.055m_0 obtained very recently by Goiran *et al.*[2] using electron cyclotron resonance, although we note that initial calculations using higher values of the effective mass produced very similar results. The other parameters used in the calculation are listed in Table II. We note that our approach calculates the drift mobility, whereas the Hall mobility is the measured quantity. However, we expect the Hall factor for the degenerate electron concentrations in the experimentally studied films to be very close to 1.[29] We also note that for the Seebeck coefficient calculations, we did not include phonon drag effects as we do not expect to observe them in the experimental temperature range.

It is interesting to compare the energy dependence of the lifetime τ for ionized impurity (ii) and charged dislocation (dis) scattering in the context of the form used for the relaxation time approximation $\tau = \tau_0(\frac{\varepsilon}{k_B T})^r$ where ε is the electron energy, k_B is Boltzmann's constant, and T is the temperature. For nondegenerate electron concentrations, $r = +3/2$ for both mechanisms, which is the textbook result for ii scattering.[49] However, at the degenerate electron concentrations found in InN films, the power dependence of the scattering for the different mechanisms is altered. This is illustrated in Fig. 1 for an electron concentration of 4×10^{17} cm^{-3}, corresponding to the low end of the films evaluated experimentally in this study. The relationship between τ and ε is no longer a strict power law, but, more importantly, the slope, which can be considered an effective value of r, is always steeper for dislocation scattering. The difference becomes even more pronounced with strong screening at higher electron concentrations.

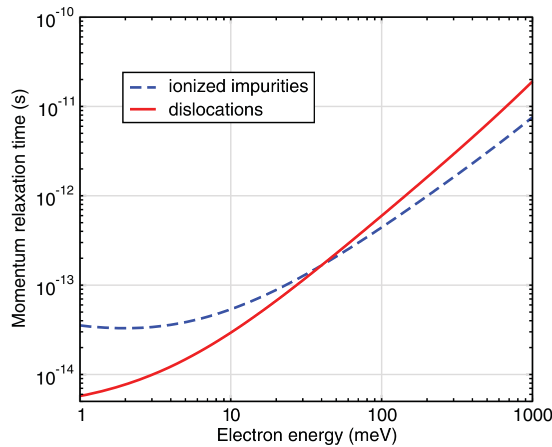

FIG. 1. (Color online) Comparison of momentum relaxation times $\tau = \nu^{-1}$ for ionized impurity (ii) and charged dislocation (dis) scattering as a function of electron energy ε for an electron concentration of 4×10^{17} cm^{-3} and a dislocation density of 1×10^{9} cm^{-2}. Under these conditions, the Fermi level at 300 K is 11 meV. At higher energies, the relationship is approximately a power law with $r = 1.1$ for ii and 1.4 for dis. At lower electron energies, the scattering time becomes less dependent on electron energy, but the slope (effective value of r) is always steeper for dis.

Insight into how the balance of charged dislocations versus ionized point impurities will affect the thermopower can be gained from the form for S in the relaxation time approximation (i.e., ignoring LO phonon scattering, which is an inelastic mechanism) in the nondegenerate limit

$$S_{\text{nondegen}} = -\frac{k_B}{|e|}\left(r + \frac{5}{2} - \frac{\zeta}{k_B T}\right), \quad (1)$$

where e is the electron charge and ζ is the Fermi level measured with respect to the conduction-band edge (negative for the nondegenerate case). A larger value of r, as predicted for dis vs ii scattering, would be expected to produce a larger absolute value of the Seebeck coefficient at the same electron concentration for this nondegenerate case. We show below that this is true for the degenerate case as well.

It is also interesting to compare the effects on the calculated thermopower and mobility produced by dislocation scattering as opposed to compensation and/or multiply charged point defects. As prior studies have shown, compensation effectively increases the strength of the ionized impurity scattering mechanism, which tends to flatten the T dependence of μ in the direction of what is experimentally observed.[46] Similarly, if the point defects are multiply charged, for example with $Z = +3$, the strength of the ii mechanism increases as the relaxation rate scales as Z^2.[50] However, as shown in Fig. 2, the effect on the thermopower is much less pronounced, because, as discussed above, the effective r of the dominant scattering mechanism is not changed.

In their treatment of negatively charged dislocations in GaN, Look and Sizelove assumed the charge to be distributed continuously along the line at a rate of one charge per c lattice constant distance.[21] Subsequent work on GaN has produced estimates in the range of 0.3–1e per c lattice constant, depending on the type of dislocation and type (n or p) of GaN.[23,25,51] For InN, prior work has assumed one charge per

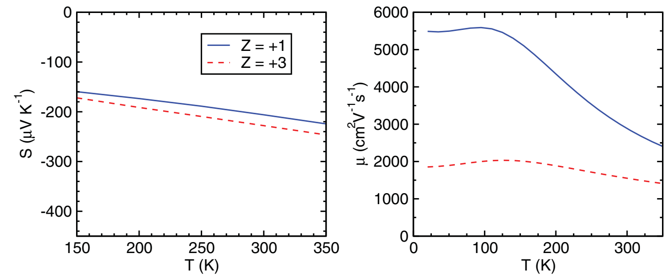

FIG. 2. (Color online) Calculated thermopower (a) and mobility (b) for $n = 4 \times 10^{17}$ cm^{-3} for uncompensated InN ($Z = +1$) and for the case of compensation or multiply charged donors $Z = +3$. Assuming that all electrons come from triply charged donors is equivalent to assuming a compensation ratio N_A/N_D of 0.5; i.e., $N_A = 4 \times 10^{17}$ cm^{-3} and $N_D = 8 \times 10^{17}$ cm^{-3} and full ionization.

monolayer along threading dislocations.[13,28] Here we will assume the same value, noting that this assumption does not change the dislocation scattering mechanism but just the dislocation densities we will extract from our analysis. If the dislocations are singly charged and positive (donors), the following charge neutrality relation is in effect:

$$n + N_A = N_D + N_{\text{dis}}/c, \quad (2)$$

where c is the lattice constant in the c direction along the dislocation line, N_D and N_A are the donor and acceptor concentrations, respectively, and N_{dis} is the charged dislocation density. If the dislocations are acceptors, N_{dis} will appear of the left-hand side of Eq. (2). Finally, per the discussion above, we will assume that $N_A \ll N_D$ and full ionization of all donors (due to the degenerate nature of the film). Thus, with a given value of n, we can vary N_{dis} to fit the experimental transport data, obtaining N_D from the charge neutrality relation, Eq. (2).

The predicted effect of dislocation scattering on mobility is dramatic. The calculated mobility of InN at room temperature as a function of dislocation density N_{dis} is shown in Fig. 3

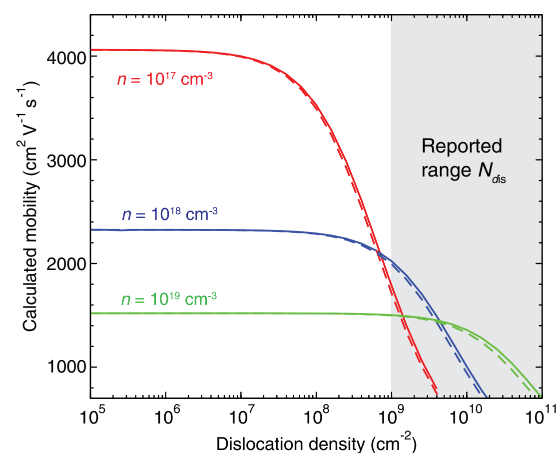

FIG. 3. (Color online) Calculated dependence of mobility on dislocation density for three different values of electron concentration, 10^{17}–10^{19} cm^{-3} (solid lines, donor dislocations; dashed lines, acceptor dislocations). The ionized impurity concentration was determined from the charge neutrality condition in Eq. (2) (see text). The shaded region indicates the range of typical dislocation densities reported in the literature for InN.

for several values of the electron concentration n. Donor and acceptor-like dislocations were considered; the predicted mobility is slightly lower for acceptor dislocations because a higher concentration of ionized point defects is required to maintain charge neutrality. A dislocation-density threshold exists, below which the mobility is invariant to changes in N_{dis} and above which the mobility sharply declines with increasing N_{dis}. The critical threshold depends on the electron concentration and varies from $\sim 10^8$ to 10^{10} cm^{-2} for the range of n considered here, taking on a larger value for higher electron concentrations. This is because a greater density of mobile charges is more effective at screening the charged dislocations, thereby minimizing their deleterious effects until there are more of them. This figure also shows that the typical range of N_{dis} reported in the literature is high enough to affect the mobility, especially for films with $n < 10^{18}$ cm^{-3}.

IV. RESULTS AND DISCUSSION

The measured Seebeck coefficients at 300 K are shown in Fig. 4 for 13 InN films. As expected for n-type material, the Seebeck coefficients are negative and $|S|$ decreases with increasing n. However, for similar n, S shows considerable variance. Also shown in Fig. 4 are model calculations of S using a charged dislocation range of 0–10^{12} cm^{-2}. As discussed above, due to the stronger dependence of the relaxation rates on energy for charged dislocation versus ionized impurity scattering, an increased proportion of dislocation scattering increases $|S|$. Nearly all of the data points can be explained using $N_{\text{dis}} \leqslant 10^{11}$ cm^{-2}.

The measured Seebeck coefficient and mobility as a function of temperature for the three films selected for detailed study are shown in Fig. 5. The room-temperature values are also shown in Table I. Here we see that electron mobility is nearly temperature invariant for the higher carrier concentration samples A and B and only for sample C, with carrier concentration approaching 10^{17} cm^{-3}, does the mobility change significantly with temperature, reaching a maximum value near 150 K.

The nearly temperature invariant mobility has been reported previously for InN,[20] but its microscopic origin had not been completely understood. Use of the standard scattering formalism for III-V's overestimates the mobility and predicts a much stronger temperature dependence, as shown by the dashed line in Fig. 5 for sample C. However, adding the charged dislocation scattering mechanism and using N_{dis} primarily and also n, subject to the charge neutrality relation in Eq. (2), produces good agreement between the calculated and measured values of Seebeck coefficient and mobility as a function of temperature. Good fits to the experimental mobility

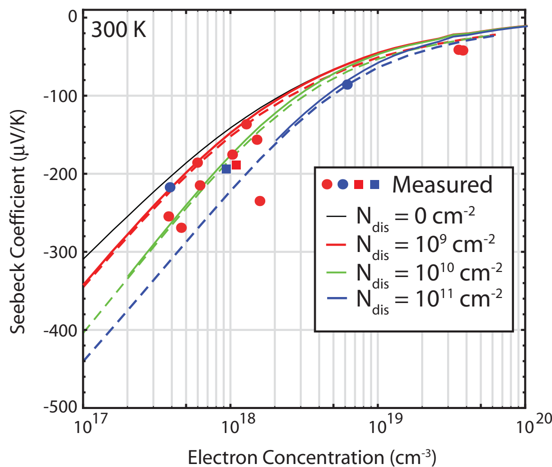

FIG. 4. (Color online) Measured values of the room-temperature Seebeck coefficient as a function of electron concentration n for 14 InN films with thicknesses between 128 nm and 12.2 μm. Circles are for films grown at Cornell; squares are for films grown at UCSB. Samples used in the TEM analysis are indicated by blue symbols. Lines are calculated values for a charged dislocation density N_{dis} in the range of 10^9–10^{11} cm^{-2}. Solid lines are for donor dislocations; dashed line assume that they are acceptors.

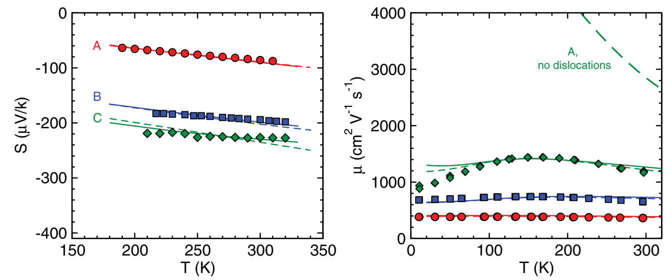

FIG. 5. (Color online) Measured (points) and modeled (lines) Seebeck coefficient (a) and mobility (b) of selected samples A, B, and C as a function of temperature. Solid lines were obtained assuming that the dislocations are donors; for dashed lines, acceptor-like dislocations were assumed (see text). The dislocation densities used to obtain the best fit are shown in Table III. In (b), the thick dashed line indicates the modeled mobility for sample C (lowest n and highest μ of the films in this study) without dislocation scattering, i.e., with $N_D = n$. Without charged dislocation scattering, the modeled mobility is too large and does not reproduce the observed relatively flat temperature response.

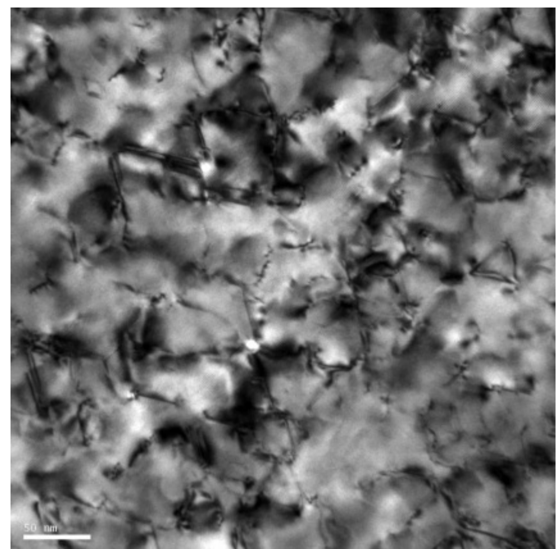

FIG. 6. Plan-view TEM image of sample A. Most of the contrast in this image comes from dislocations. The dislocation density is estimated to be on the order of 10^{11} cm^{-2}.

TABLE III. Results of self-consistent modeling of variable temperature Hall-effect and Seebeck coefficient measurements using n and N_{dis} as parameters. Fit values obtained assuming that the dislocations are donors are in the first line for each sample; values obtained assuming that the dislocations are acceptors are in the second line in parentheses. The values of n measured by Hall effect and the range of dislocation densities measured by TEM (see text) are also shown, as is the fraction of the total carriers stemming from dislocations if they are assumed to be donors.

	n (cm^{-3})		N_{dis} (cm^{-2})		
Sample	Measured	Model	Measured	Model	Fraction of n from N_{dis}
A (GS1360)	6×10^{18}	6.5×10^{18} (6.5×10^{18})	$\sim 1 \times 10^{11}$	1.5×10^{11} (1.5×10^{11})	0.49
B (100907AC)	9×10^{17}	8.0×10^{17} (7.6×10^{17})	2–5 $\times 10^{10}$	1.5×10^{10} (1.3×10^{10})	0.33
C (GS2060)	4×10^{17}	4.8×10^{17} (4.6×10^{17})	$\sim 1 \times 10^{9}$–5×10^{10}	4.1×10^{9} (3.9×10^{9})	0.15

data can be obtained for both possibilities for the charge state of the dislocations: donors or acceptors. Fits to the Seebeck coefficient are very similar for both cases, except for sample C with the lowest electron concentration. For this sample, the temperature dependence of S is in better correspondence with the experimental data, assuming the dislocations are donors. The best-fit n and dislocation densities are summarized in Table III; the value of n used in the fitting and that measured with Hall effect are in good agreement.

If the dislocations are donors, it is interesting to consider what contribution this makes to the overall electron concentration in the films. The fraction of n which is predicted to come from dislocations acting as donors is also given in Table III; this fraction is between 14% and 44%. Although we do not have systematic impurity concentration data for these films, this observation could be seen to be consistent with literature reports that have reported a correlation of n with dislocation density in some films. Finally, we note that the model predicts a higher low temperature mobility for Sample C, which has the lowest electron concentration of the films in this study. It is possible in this case that there is additional scattering from random electrostatic and strain potentials, some of which might be due to a nonuniform distribution of dopants and/or dislocations.[46] Scattering by neutral impurities is another possibility.

The dislocation density was evaluated by TEM for comparison to the modeling results. Prior work has found that the dislocation density is often nonuniform through the thickness of InN films.[17] Typically, the dislocation density drops rapidly within the first few hundred nanometers of film growth before reaching a constant value. Sample A is sufficiently thin such that the dislocation density has not reached the typical asymptotic value. As shown in Fig. 6, the surface dislocation density measured in plan view is $\sim 10^{11}$ cm^{-2}. This is in

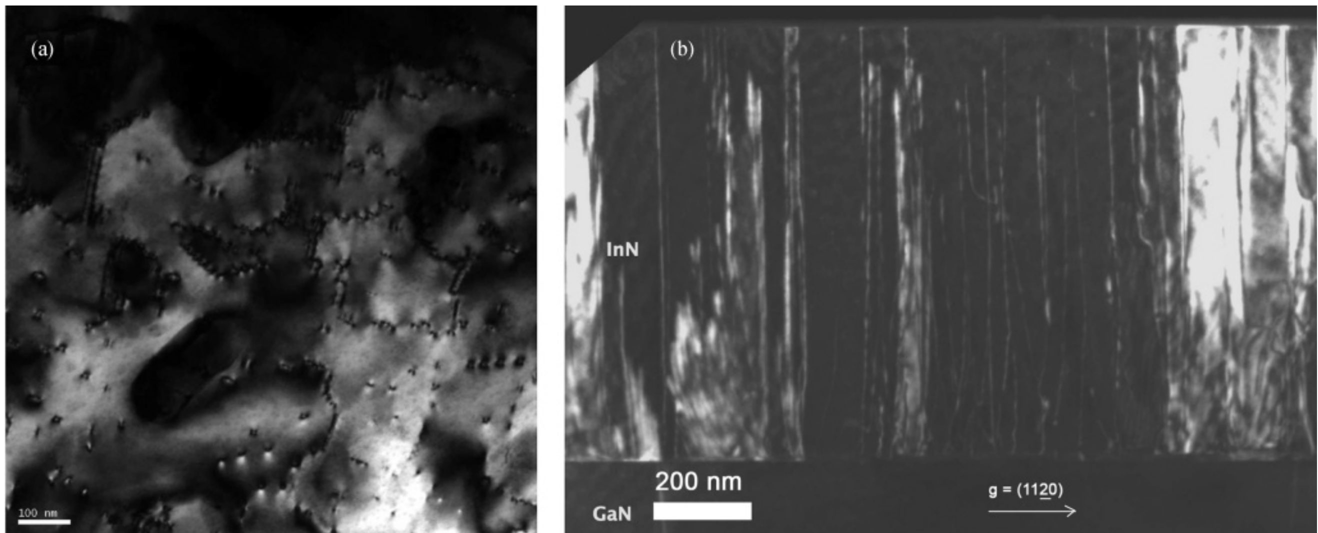

FIG. 7. Plan-view (a) and cross-sectional (b) TEM images of sample B. The surface dislocation density was estimated from several plan images and is 2×10^{10} cm^{-2}. The pattern of dislocations is interesting; they form in lines stitching out a patchwork of areas that are largely dislocation free. This implies that the growth began as three-dimensional islands, which later coalesced requiring dislocations to accommodate the low-angle grain boundaries. The dislocation types are estimated to be ∼1/3 mixed type, ∼2/3 pure edge, and $<10\%$ screw. The cross-section image in (b) indicates that the dislocation density does not vary substantially through the thickness of this film. With the indicated contrast condition, the concentration of pure edge and/or mixed character dislocations is on the order of 5×10^{10} cm^{-2}.

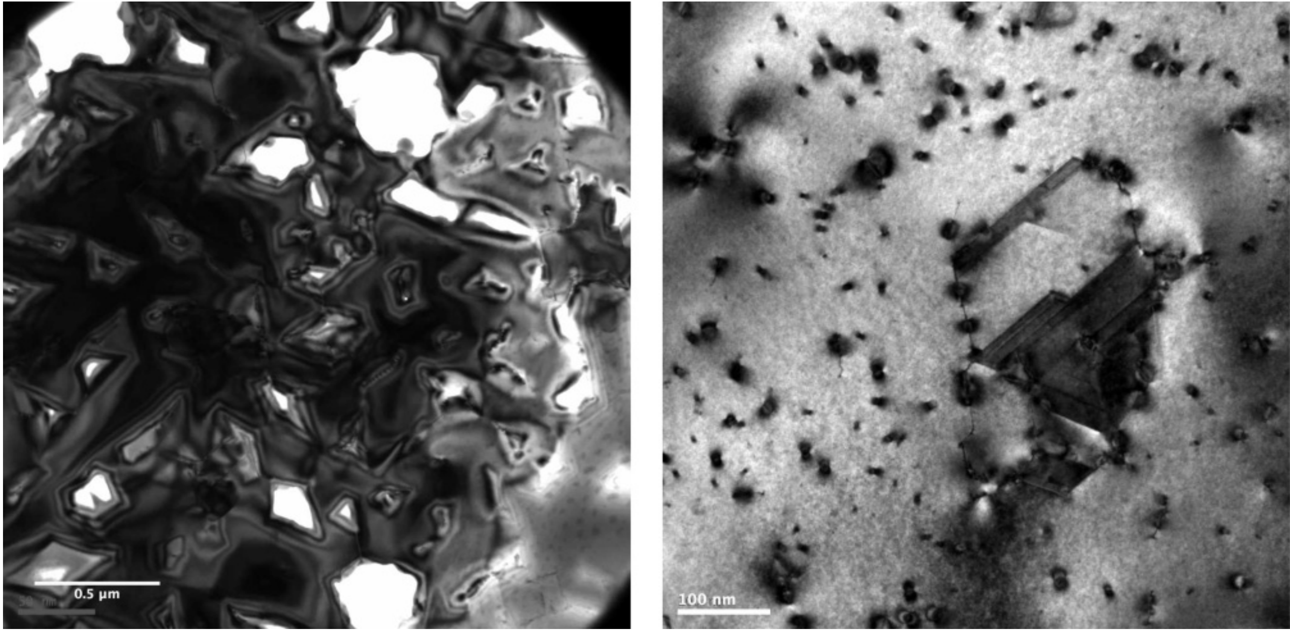

FIG. 8. Surface plan-view (a) and mid-film plan-view (b) TEM images of sample C. Dislocation density at surface, averaged from several images, appears to be as low as 1×10^9 cm^{-2} although the roughness of the films and the pits which form in the foil as a result add some uncertainty to this determination. The mid-layer dislocation density determined from the image in (b) and several other images is $\sim 5 \times 10^{10}$ cm^{-2}, similar to the values found throughout sample B. However, in contrast to sample B, the dislocations do not appear to be distributed along grain boundaries.

good agreement with the dislocation density obtained from the modeling (see Table III). TEM images from sample B are shown in Fig. 7. In this case, the film is sufficiently thick, 1 μm, so that dislocation density has a constant value throughout most of the film thickness, $\sim 5 \times 10^{10}$ cm^{-2}. This measured value is fairly typical of high-quality, metal polar, *c*-axis oriented, InN films grown heteroepitaxially on GaN buffers. It is on the order of but larger than the value obtained from the transport modeling; this may indicate that not all of the dislocations are ionized. Sample C (Fig. 8) is very thick, 12.2 μm. At mid-film, the dislocation density appears similar to that of Sample B. At the film surface, the dislocation could be very low, on the order of what is derived from the transport analysis (in the 10^9 cm^{-2} range). However, the rough surface of the film (this is expected for such a thick growth) and the resultant pits which arise in the TEM foil as a result add some uncertainty to the quantitative measurement. The charged dislocation density obtained from the transport modeling is in the mid-10^9 cm^{-2} range. Considering that the Hall-effect measurement is weighted by the square of the mobility of the carriers, which weights transport measurements toward low-dislocation-density parts of the film since high-dislocation-density parts of the film have lower mobility, the modeled value seems consistent with the range of N_{dis} obtained from the TEM analysis.

V. CONCLUSIONS

We have shown that the inclusion of electron scattering by charged line defects allows the weak temperature dependence of the electron mobility in InN films to be explained. Moreover, measuring both the Hall effect and Seebeck coefficient as a function of temperature and modeling the results with solutions to the Boltzmann transport equation, we have shown that it is possible to evaluate the charged dislocation density. The values obtained from this analysis are in good correspondence with independent TEM measurements of the threading dislocation density over two orders of magnitude, providing evidence that dislocations strongly affect transport in n-type InN films. The transport measurements by themselves cannot determine whether the charged dislocations are donors or acceptors.

This work shows that in order to achieve the predicted high electron mobilities in InN, the dislocation density will need to be lowered by at least an order of magnitude from the current "state of the art" of $\sim 10^9$ cm^{-2}. Also, if the dislocations are donors and provide one electron per unit cell, the dislocation density provides a lower limit to n; i.e., a charged dislocation density of 10^9 cm^{-2} corresponds to an electron density of 2×10^{16} cm^{-3}. Finally, the charge accumulation that would be expected to occur around charged line defects has important implications as well; it is possible that vertical conduction along threading dislocations is one reason that pn junctions in InN have been hard to produce, in spite of recent reports confirming p-type conduction in Mg-doped InN films.[14,52–54]

ACKNOWLEDGMENTS

This work was performed within LBNL's Electronic Materials Program. Electron microscopy was performed at the National Center for Electron Microscopy. Both are supported by the Director, Office of Science, Office of Basic Energy Sciences, Division of Materials Sciences and Engineering, of

the US Department of Energy under Contract Nos. DE-AC02-05CH11231. N.M. was supported by the National Defense Science and Engineering Graduate (NDSEG) program of the Department of Defense, Air Force Office of Scientific Research.

APPENDIX

1. Momentum relaxation rates

The momentum relaxation rates $\nu(k)$ for the different scattering mechanisms, where k is the electron momentum, can be found in many textbooks (e.g., Ref. 49; we used the forms provided by Rode[39]). Of relevance here are the differences between scattering by point charges and line charges. For scattering by line charges (dislocations) we used the form adapted by Look and Sizelove[21] for calculating the effect of dislocations on mobility in GaN. This form for the scattering rate was first developed by Pödör[55] based on a potential for electron scattering from screened line charges derived by Bonch-Bruevich and Glasko.[56] It is

$$\nu_{\mathrm{dis}}(k) = \frac{N_{\mathrm{dis}} m_e^* e^4}{\hbar^3 \varepsilon_S^2 c^2}\left[\beta^4\left(1+\frac{4k^2}{\beta^2}\right)^{3/2}\right]^{-1}, \quad \text{(A1)}$$

where m_e^* is the (k-dependent, see below) electron effective mass, ε_S is the static dielectric constant, c is the lattice constant, and β is the inverse screening length

$$\beta^2 = \frac{e^2}{\varepsilon_S k_{\mathrm{B}} T}\int\left(\frac{k}{\pi}\right)^2 f_0(1-f_0)dk, \quad \text{(A2)}$$

where f_0 is the Fermi-Dirac equilibrium distribution function. In the degenerate and nondegenerate limits, β is the inverse Debye length and inverse Thomas-Fermi screening length, respectively. The electron scattering rate for both point and line defects does not depend on the charge state (+ or −) of the defect.

2. Conduction-band dispersion

In Eq. (A1), and in all other relaxation rate calculations which involve the electron effective mass, we accounted for its energy dependence due to the nonparabolic conduction band of InN using the two-band $\mathbf{k}\cdot\mathbf{p}$ in the limit of negligible spin-orbit splitting Δ to calculate the conduction-band dispersion[39,57]

$$\varepsilon(k) = \frac{\hbar^2 k^2}{2m_0} + \frac{\varepsilon_g(\alpha-1)}{2}, \quad \text{(A3)}$$

where α is defined as

$$\alpha^2(k) = 1 + \frac{2\hbar^2 k^2}{m_0 \varepsilon_g}\left(\frac{m_0}{m_{e,0}^*}-1\right), \quad \text{(A4)}$$

and ε_g is the band gap. Using Eq. (A3) with the electron momentum at the Fermi level k_{F} yields an effective mass range of $0.056m_0$ ($n = 4\times10^{17}$ cm^{-3}, $k_{\mathrm{F}} = 0.13$ nm^{-1}) to $0.12m_0$ ($n = 5\times10^{19}$ cm^{-3}, $k_{\mathrm{F}} = 1.1$ nm^{-1}) with a band-edge effective mass $m_{e,0}^* = 0.055m_0$ ($k_{\mathrm{F}} = 0$ nm^{-1}).

3. Boltzmann transport equation

Our modeling is based on solving the linearized Boltzmann transport equation

$$f(\boldsymbol{k}) = f_0(k) + xg(k), \quad \text{(A5)}$$

where $f(\boldsymbol{k})$ is the total momentum distribution function, $k = |\boldsymbol{k}|$, x is the cosine of the angle between the small driving force (electric field or temperature gradient in our case), and $g(k)$ is the perturbation part of the distribution.[39,49] In the relaxation time approximation, and when the driving force is an electrical field F,

$$g(k) = -\frac{eF}{\hbar\nu_{\mathrm{el}}}\frac{\partial f_0}{\partial k}, \quad \text{(A6)}$$

where ν_{el} is the sum of the elastic relaxation scattering rates, the most relevant of which for this analysis, ionized impurity and charged dislocation scattering, are described above. The addition of LO phonon scattering, an inelastic process, requires an iterative procedure to determine g.[38,39] Once $g(k)$ is determined, the drift mobility μ is calculated by integrating over k:

$$\mu = \frac{\hbar}{3}\frac{\int k^3 \frac{g(k)}{Fm_e^*}dk}{\int k^2 f_0 dk}. \quad \text{(A7)}$$

While the use of the Rode method for calculating drift mobility is well documented in the literature, use of this method to calculate thermopower is less-well developed.[58] It is a two-step procedure. First, the current density J is calculated in the presence of a temperature gradient $\frac{\partial T}{\partial z}$. The driving force is different than for the calculation of the mobility; this is most easily seen in the form obtained for g in the relaxation time approximation for a nondegenerate parabolic band:

$$g(k) = \frac{-v(k)}{\nu_{\mathrm{el}}}\frac{\partial f_0}{\partial z}, \quad \text{(A8)}$$

where $v(k)$ is the electron velocity k/m_e^* and $\partial f_0/\partial z$ is

$$\frac{\partial f_0}{\partial z} = f_0(1-f_0)\left[\frac{\varepsilon(k)}{k_{\mathrm{B}}T} - \frac{\int k^2 f_0(1-f_0)\frac{\varepsilon(k)}{k_{\mathrm{B}}T}dk}{\int k^2 f_0(1-f_0)dk}\right]\frac{1}{T}\frac{\partial T}{\partial z}. \quad \text{(A9)}$$

Again, an iterative procedure is required to obtain g when inelastic scattering is considered. An integral over k is used to obtain J (this is essentially the Peltier current):

$$J = \frac{\hbar e}{3\pi^2}\int k^3\frac{g(k)}{m_e^*}dk. \quad \text{(A10)}$$

Finally, the Seebeck coefficient S is given by

$$S = -\left(\frac{\partial\varepsilon_F}{\partial z}\Big/ e + \frac{J}{\sigma}\right)\Big/\frac{\partial T}{\partial z}, \quad \text{(A11)}$$

where the appearance of the electrical conductivity $\sigma = en\mu$ implies that the drift mobility also needs to be calculated using the procedure described above. The first term in (A11) with the temperature gradient divided out is

$$\frac{k_{\mathrm{B}}}{e}\left[\frac{\int k^2 f_0(1-f_0)\frac{\varepsilon(k)}{k_{\mathrm{B}}T}dk}{\int k^2 f_0(1-f_0)dk} - \frac{\zeta}{k_{\mathrm{B}}T}\right]. \quad \text{(A12)}$$

*JWAger@lbl.gov

[1] W. Walukiewicz, J. W. Ager, III, K. M. Yu, Z. Liliental-Weber, J. Wu, S. X. Li, R. E. Jones, and J. D. Denlinger, J. Phys. D **39**, R83 (2006).
[2] M. Goiran, M. Millot, J. M. Poumirol, I. Gherasoiu, W. Walukiewicz, and J. Leotin, Appl. Phys. Lett. **96**, 052117 (2010).
[3] V. M. Polyakov and F. Schwierz, Appl. Phys. Lett. **88**, 032101 (2006).
[4] Z. Yarar, Phys. Status Solidi B **244**, 3711 (2007).
[5] J. Wu, J. Appl. Phys. **106**, 011101 (2009).
[6] A. G. Bhuiyan, A. Hashimoto, and A. Yamamoto, J. Appl. Phys. **94**, 2779 (2003).
[7] C. S. Gallinat, G. Koblmüller, J. S. Brown, S. Bernardis, J. S. Speck, G. D. Chern, E. D. Readinger, H. Shen, and M. Wraback, Appl. Phys. Lett. **89**, 032109 (2006).
[8] C. S. Gallinat, G. Koblmüller, and J. S. Speck, Appl. Phys. Lett. **95**, 022103 (2009).
[9] V. Darakchieva, K. Lorenz, N. P. Barradas, E. Alves, B. Monemar, M. Schubert, N. Franco, C. L. Hsiao, L. C. Chen, W. J. Schaff, L. W. Tu, T. Yamaguchi, and Y. Nanishi, Appl. Phys. Lett. **96**, 081907 (2010).
[10] E. A. Davis, S. F. J. Cox, R. L. Lichti, and C. G. Van de Walle, Appl. Phys. Lett. **82**, 592 (2003).
[11] A. Janotti, and C. G. Van de Walle, Appl. Phys. Lett. **92**, 032104 (2008).
[12] L. F. J. Piper, T. D. Veal, C. F. McConville, H. Lu, and W. J. Schaff, Appl. Phys. Lett. **88**, 252109 (2006).
[13] X. Wang, S. B. Che, Y. Ishitani, and A. Yoshikawa, Appl. Phys. Lett. **90**, 151901 (2007).
[14] H. Wang, D. S. Jiang, L. L. Wang, X. Sun, W. B. Liu, D. G. Zhao, J. J. Zhu, Z. S. Liu, Y. T. Wang, S. M. Zhang, and H. Yang, J. Phys. D: Appl. Phys. **41**, 135403 (2008).
[15] C. J. Lu, L. A. Bendersky, H. Lu, and W. J. Schaff, Appl. Phys. Lett. **83**, 2817 (2003).
[16] D. Muto, H. Naoi, T. Araki, S. Kitagawa, M. Kurouchi, H. Na, and Y. Nanishi, Phys. Status Solidi A **203**, 1691 (2006).
[17] V. Lebedev, V. Cimalla, J. Pezoldt, M. Himmerlich, S. Krischok, J. A. Schaefer, O. Ambacher, F. M. Morales, J. G. Lozano, and D. González, J. Appl. Phys. **100**, 094902 (2006).
[18] T. Akagi, K. Kosaka, S. Harui, D. Muto, H. Naoi, T. Araki, and Y. Nanishi, J. Electron. Mater. **37**, 603 (2008).
[19] D. C. Look, C. E. Stutz, R. J. Molnar, K. Saarinen, and Z. Liliental-Weber, Solid State Commun. **117**, 571 (2001).
[20] V. Lebedev, V. Cimalla, T. Baumann, O. Ambacher, F. M. Morales, J. G. Lozano, and D. González, J. Appl. Phys. **100**, 094903 (2006).
[21] D. C. Look and J. R. Sizelove, Phys. Rev. Lett. **82**, 1237 (1999).
[22] D. Cherns and C. G. Jiao, Phys. Rev. Lett. **87**, 205504 (2001).
[23] E. Müller, D. Gerthsen, P. Brückner, F. Scholz, T. Gruber, and A. Waag, Phys. Rev. B **73**, 245316 (2006).
[24] P. J. Hansen, Y. E. Strausser, A. N. Erickson, E. J. Tarsa, P. Kozodoy, E. G. Brazel, J. P. Ibbetson, U. Mishra, V. Narayanamurti, S. P. DenBaars, and J. S. Speck, Appl. Phys. Lett. **72**, 2247 (1998).
[25] A. Krtschil, A. Dadgar, and A. Krost, Appl. Phys. Lett. **82**, 2263 (2003).
[26] H. Choi, E. K. Koh, Y. M. Cho, J. Jin, D. Byun, and M. Yoon, Microelectron. J. **36**, 25 (2005).
[27] P. Ebert, L. Ivanova, S. Borisova, H. Eisele, A. Laubsch, and M. Dähne, Appl. Phys. Lett. **94**, 062104 (2009).
[28] D. C. Look, H. Lu, W. J. Schaff, J. Jasinski, and Z. Liliental-Weber, Appl. Phys. Lett. **80**, 258 (2002).
[29] K. A. Wang, Y. Cao, J. Simon, J. Zhang, A. Mintairov, J. Merz, D. Hall, T. Kosel, and D. Jena, Appl. Phys. Lett. **89**, 162110 (2006).
[30] X.-G. Yu and X.-G. Liang, J. Appl. Phys. **103**, 043707 (2008).
[31] Y. Takei and T. Nakayama, J. Cryst. Growth **311**, 2767 (2009).
[32] H. Lu, W. J. Schaff, J. Hwang, H. Wu, W. Yeo, A. Pharkya, and L. F. Eastman, Appl. Phys. Lett. **77**, 2548 (2000).
[33] H. Lu, W. J. Schaff, J. Hwang, H. Wu, G. Koley, and L. F. Eastman, Appl. Phys. Lett. **79**, 1489 (2001).
[34] C. S. Gallinat, G. Koblmüller, J. S. Brown, and J. S. Speck, J. Appl. Phys. **102**, 064907 (2007).
[35] G. Koblmüller, C. S. Gallinat, and J. S. Speck, J. Appl. Phys. **101**, 083516 (2007).
[36] J. W. Ager, III, N. Miller, R. E. Jones, K. M. Yu, J. Wu, W. J. Schaff, and W. Walukiewicz, Phys. Status Solidi B **245**, 873 (2008).
[37] N. Miller, Ph.D. thesis, University of California, Berkeley, 2010.
[38] D. L. Rode, Phys. Rev. B **2**, 1012 (1970).
[39] D. L. Rode, in *Semiconductors and Semimetals*, edited by R. K. Willardson and A. C. Beer (Academic Press, New York, 1975), Vol. 10, pp. 1–89.
[40] J. Wu, W. Walukiewicz, W. Shan, K. M. Yu, J. W. Ager, III, E. E. Haller, H. Lu, and W. J. Schaff, Phys. Rev. B **66**, 201403 (2002).
[41] S. P. Fu and Y. F. Chen, Appl. Phys. Lett. **85**, 1523 (2004).
[42] T. Inushima, K. Fukui, H. Lu, and W. J. Schaff, Appl. Phys. Lett. **92**, 171905 (2008).
[43] A. Kasic, M. Schubert, Y. Saito, Y. Nanishi, and G. Wagner, Phys. Rev. B **65**, 115206 (2002).
[44] T. Inushima, M. Higashiwaki, and T. Matsui, Phys. Rev. B **68**, 235204 (2003).
[45] Y.-M. Chang, H. W. Chu, C.-H. Shen, H.-Y. Chen, and S. Gwo, Appl. Phys. Lett. **90**, 072111 (2007).
[46] L. Hsu, R. E. Jones, S. X. Li, K. M. Yu, and W. Walukiewicz, J. Appl. Phys. **102**, 073705 (2007).
[47] P. Schley, R. Goldhahn, G. Gobsch, M. Feneberg, K. Thonke, X. Wang, and A. Yoshikawa, Phys. Status Solidi B **246**, 1177 (2009).
[48] M. A. Moram and M. E. Vickers, Rep. Prog. Phys. **72**, 036502 (2009).
[49] K. Seeger, *Semiconductor Physics* (Springer, New York, 2002).
[50] R. E. Jones, S. X. Li, L. Hsu, K. M. Yu, W. Walukiewicz, Z. Liliental-Weber, J. W. Ager, III, E. E. Haller, H. Lu, and W. J. Schaff, Physica B **366–377**, 436 (2006).
[51] J. Cai and F. A. Ponce, Phys. Status Solidi A **192**, 407 (2002).
[52] R. E. Jones, K. M. Yu, S. X. Li, W. Walukiewicz, J. W. Ager, III, E. E. Haller, H. Lu, and W. J. Schaff, Phys. Rev. Lett. **96**, 125505 (2006).
[53] L. H. Dmowski, M. Baj, T. Suski, J. Przybytek, R. Czernecki, X. Wang, A. Yoshikawa, H. Lu, W. J. Schaff, D. Muto, and Y. Nanishi, J. Appl. Phys. **105**, 123713 (2009).
[54] N. Miller, J. W. Ager, III, H. M. Smith, III, M. A. Mayer, K. M. Yu, E. E. Haller, W. Walukiewicz, W. J. Schaff, C. Gallinat, G. Koblmüller, and J. S. Speck, J. Appl. Phys. **107**, 113712 (2010).
[55] B. Pödör, Phys. Status Solidi B **16**, K167 (1966).
[56] V. L. Bonch-Bruevich and V. B. Glasko, Fiz. Tverd. Tela **3**, 36 (1961).
[57] E. O. Kane, J. Phys. Chem. Solids **1**, 249 (1957).
[58] D. L. Rode, Phys. Rev. B **3**, 3287 (1971).